ORIGINAL RESEARCH ARTICLE

Effect of Milling Time on the Structural and Magnetic Properties of Nanostructured $Fe_{90}Si_{10}$ Alloys

Abderrahmane Younes[1] · Rachid Amraoui[1] · Amirouche Bouamer[1] · Mounia Guessoum[1] · Zoheir Boutaghou[1] · Fatiha Smaili[1] · Asmaa Mendoud[1]

Abstract

Nanostructured $Fe_{90}Si_{10}$ powders were synthesized through a mechanical alloying process to explore the impact of milling duration on both their magnetic behavior and structural properties. Our investigation involved a comprehensive analysis encompassing morphological, magnetic, and structural characterizations, employing scanning electron microscopy (SEM) coupled with energy-dispersive x-ray spectroscopy (EDS), a vibrating sample magnetometer, and x-ray diffraction (XRD). XRD analysis unveiled the formation of a disordered $Fe_{90}Si_{10}$ solid solution exhibiting a body-centered cubic crystal structure after 15 h of milling. With increasing milling time, the lattice parameter gradually increased from 0.2861 nm for the unmilled $Fe_{90}Si_{10}$ powder to 0.4528 nm after 30 h of milling. The sample subjected to 30 h of milling revealed an average crystallite size of 19.51 ± 0.03 nm, accompanied by noteworthy lattice deformation ($0.236 \pm 0.006\%$). To assess morphological evolution and elemental composition homogeneity during milling, SEM and EDS analyses were employed, respectively. For nanostructured $Fe_{90}Si_{10}$, we examined coercivity (H_c), magnetization saturation (M_s), remanent magnetization (M_r), and squareness (M_r/M_s) as functions of milling time through hysteresis loop measurements. The highest values for H_c, M_s, M_r, and M_r/M_s were achieved after 30 h. This study elucidates the intricate relationship between mechanical milling duration and the magnetic and structural properties of nanostructured $Fe_{90}Si_{10}$, providing valuable insights into their potential applications across various fields.

Keywords Nanostructured $Fe_{90}Si_{10}$ alloy · magnetic characteristics · structural attributes · VSM analysis · XRD insights · SEM observations

Introduction

Nanostructured materials are produced using various techniques, each offering unique advantages for tailoring material properties compared to bulk materials with identical elemental compositions.[1–3] The sol–gel method is another technique used for producing nanomaterials, involving the conversion of a solution (sol) into a gel-like material (gel) and then into a solid nanomaterial through chemical reactions.[4] Chemical precipitation is a technique where nanomaterials are synthesized by precipitating them from a solution of precursor chemicals. The size and properties of the nanoparticles can be controlled by adjusting parameters such as temperature, pH, and concentration of reactants.[5] Electrospinning is employed to produce nanofibers by applying a high voltage to a polymer solution or melt, which then gets drawn into a fine fiber. This technique is suitable for producing nanofibers of various polymers and composite materials.[6,7]

Mechanical alloying (MA) is an effective technique for producing nanomaterials, offering advantages such as uniform element dispersion at the nanoscale, production of metastable phases, and improved material properties like strength, hardness, and magnetic characteristics.[8,9] The process involves repeated welding and fracturing of powder particles in a high-energy ball mill. Key parameters such as milling time, milling media, rotation speed, and ball-to-powder ratio significantly impact the final properties. MA has been extensively used to create Fe-based alloy nanocomposites with enhanced magnetic properties, allowing for

✉ Abderrahmane Younes
  younesabdo11@gmail.com

1   Research Center in Industrial Technologies (CRTI), P.O.
    Box 64, 16014 Cheraga, Algiers, Algeria

precise tailoring of these properties through careful control of the milling parameters.[10–15]

Nanostructured FeSi is chosen for its high saturation magnetization, low coercivity, and superior soft magnetic behavior, making it suitable for applications in magnetic sensors, transformers, and electric motors.[16–22] Nanostructuring further enhances these properties, increasing FeSi's appeal for advanced technological uses. MA is crucial in producing FeSi nanostructured powders with tailored characteristics, aiding in the development of magnetic and electronic devices.[23–25] Silicon's higher hardness and brittleness compared to iron lead to particle fracturing and the formation of lamellar structures, improving electrical resistivity and reducing eddy current losses. However, FeSi alloys with over 6.5 wt.% silicon become brittle, complicating conventional production methods.[26,27]

The purpose of this study is to synthesize nanostructured $Fe_{90}Si_{10}$ alloys with varying milling durations and investigate their magnetic properties. The primary objective is to assess how changes in milling time impact the structural properties and magnetic behavior of the alloy during MA. Advanced characterization techniques, including scanning electron microscopy (SEM), energy-dispersive x-ray spectroscopy (EDS), vibrating-sample magnetometry (VSM), and x-ray diffraction (XRD), will be utilized to analyze the morphological, structural, and magnetic characteristics of the FeSi samples. By examining the relationship between milling duration, crystal structure, and magnetic properties, this research seeks to deepen our understanding of how nanostructuring affects the performance of $Fe_{90}Si_{10}$ alloys. Ultimately, the study aims to provide insights for the development of $Fe_{90}Si_{10}$ alloys with improved magnetic properties, which could be highly beneficial for applications in magnetic devices and related fields.

Experimental Procedures

For this study, both Fe and Si powders with an average particle size of approximately 70 μm and a purity level of 99.5% were used as the initial materials. These powders were purchased from Sigma-Aldrich (USA). The milling process was conducted using a high-energy planetary ball mill (PM 400) operating at a speed of 400 rpm, with a ball-to-powder weight ratio of 1:20. Each sample had an initial powder mixture mass of 20 g. The powders were placed in a 250-ml-capacity tungsten carbide cylindrical flask along with tungsten carbide balls with diameters of 20 mm, and milling took place under an inert atmosphere. The duration of the milling process varied from 0 to 30 h (0, 15, 30) to systematically investigate its influence on the structural and magnetic properties of the resulting FeSi alloy powders. To mitigate excessive heating during milling,

a 15-min milling sequence was followed by a 15-min resting period.

The morphological and structural characteristics of the resultant alloy mixtures were meticulously analyzed using a Zeiss GeminiSEM scanning electron microscope equipped with EDS and a Panalytical X'Pert Pro x-ray diffractometer employing Cu Kα radiation, respectively. Furthermore, the magnetic behavior was systematically assessed utilizing a MicroSense vibrating sample magnetometer with a maximum applied field of 15 kOe. This comprehensive approach provides a thorough exploration of the milling-induced alterations in both the microstructure and magnetic properties of the FeSi alloy powders.

Results and Discussion

Structural Analysis

In Fig. 1, XRD diagrams depict the evolution of FeSi alloy powders over varying milling durations. Initially (0 h), the XRD pattern reveals distinctive Fe and Si peaks within the mixed powders. However, after 15 h of milling, the Si peaks disappear from the XRD pattern, indicating the incorporation of Si particles into the Fe lattice and resulting in the formation of the Fe(Si) solid solution. This observation concurs with the findings of Rodriguez et al.[28] who reported that XRD profiles of Fe−10% Si and Fe−20% Si samples ground for 10 h exhibited characteristic body-centered cubic (bcc) structure peaks indicative of Fe(Si) phases. After 30 h of milling, the Fe(Si) peaks reveal heightened broadening compared to the 15-h samples, coupled with a reduction in their intensities. Contrary to expectations based on conventional interpretations, as illustrated in Fig. 1, the broadening of the diffraction peaks does not appear significant even after an extended milling duration. This intriguing observation prompts an inquiry into the authors' rationale for the unexpected increase in peak intensity after 15 h of milling compared to the unmilled powders. In seeking a comprehensive understanding, it becomes imperative to explore the authors' proposed explanations for this unique phenomenon, considering potential factors such as changes in crystallite structure, grain boundaries, or other dynamic effects induced by the mechanical milling process.

The various structural parameters of the unmilled powder are summarized in Table I, calculated using the Scherrer formula.[29]

$$D = \frac{0.9\lambda}{\beta\cos\theta} \tag{1}$$

$$\varepsilon = \frac{\beta}{4tan\theta} \tag{2}$$

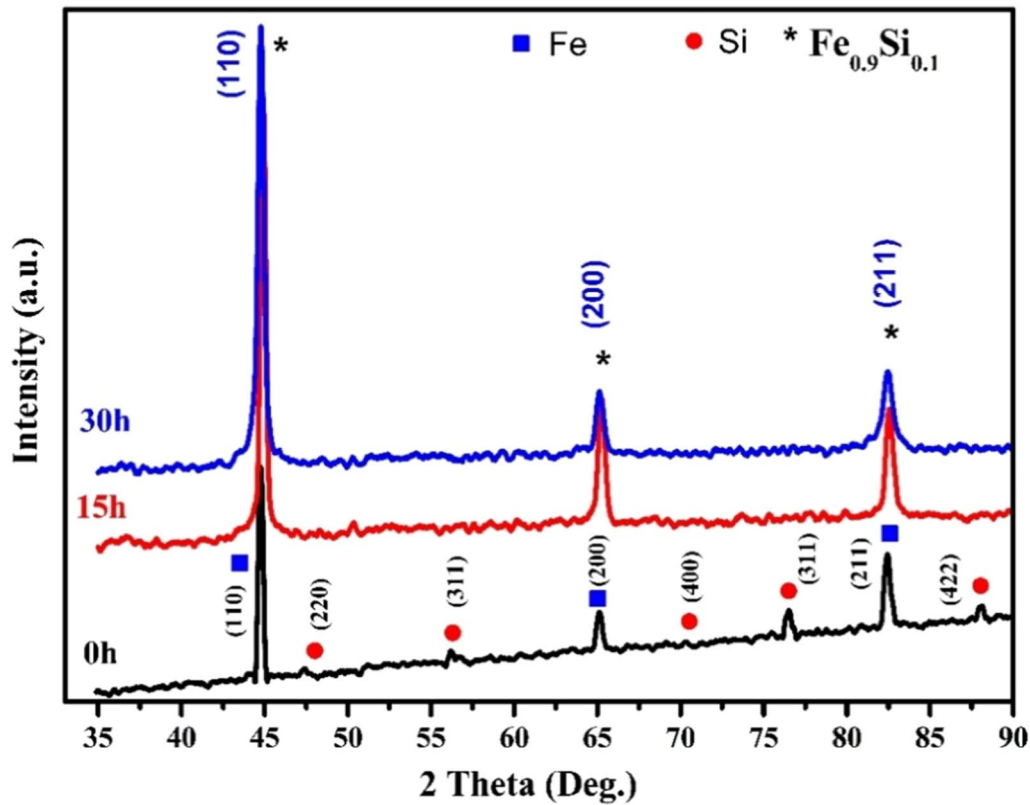**Fig. 1** XRD patterns of $Fe_{90}Si_{10}$ (wt.%) powders milled for different durations.

Table I Structural parameters of unmilled FeSi powder using the Scherrer formula

2θ (°)	β (°)	(hkl)	$d_{(hkl)}$	D (nm)	ε (%)	a (nm)
Fe						
44.75	0.319 ± 0.0159	(110)	2.0250 ± 0.101	30 ± 1.5	0.193 ± 0.009	0.2863 ± 0.01432
65.07	0.337 ± 0.0168	(200)	1.4323 ± 0.071	31 ± 1.55	0.132 ± 0.006	0.2864 ± 0.01432
82.46	0.302 ± 0.0151	(211)	1.1687 ± 0.058	39 ± 1.95	0.086 ± 0.004	0.2862 ± 0.01431
Si						
47.28	0.454 ± 0.022	(220)	1.921 ± 0.096	21 ± 1.05	0.259 ± 0.012	0.5433 ± 0.02716
56.17	0.701 ± 0.035	(311)	1.6361 ± 0.081	14 ± 0.7	0.328 ± 0.016	0.5426 ± 0.02713
69.09	0.783 ± 0.039	(400)	1.3583 ± 0.067	14 ± 0.7	0.284 ± 0.014	0.5433 ± 0.02716
76.49	0.305 ± 0.015	(331)	1.2443 ± 0.062	37 ± 1.85	0.096 ± 0.004	0.5423 ± 0.02712
88.09	0.186 ± 0.009	(422)	1.1079 ± 0.055	28 ± 1.4	0.048 ± 0.002	0.5427 ± 0.02713

The above equation was derived using the following variables: λ = 1.54059 Å (Cu radiation), β (full width at half-maximum), θ (angle in radians), and ε (lattice strain).

The changes in crystallite size, lattice strain, and lattice parameters of milled $Fe_{90}Si_{10}$ alloy powders at different milling times are presented in Table II, determined using the Williamson–Hall (W–H) formula.[30]

$$\beta \, Cos\theta = \frac{0.89\lambda}{D} + 4 \, \varepsilon Sin\theta \tag{3}$$

In this context, λ, β, θ, ε, and D represent the wavelength of Cu Kα radiation, full width at half-maximum (FWHM), Bragg angle, lattice strain, and average crystallite size, respectively.

Notably, milling time exerts a discernible influence on crystallite size and lattice parameters. As the milling time increases, a reduction in crystallite size, down to a remarkable 21.51 ± 0.03 nm, and an increase in lattice strains, reaching 0.236 ± 0.006%, become evident. These transformations are attributed to the rigorous mechanical deformation during the MA process induced by ball milling, leading to the

Table II Variation in structural parameters of $Fe_{90}Si_{10}$ during mechanical milling by the Williamson–Hall (W–H) formula

Phases	Milling time (h)	Crystallite size (nm)	Lattice strain (%)	Lattice parameter (nm)
Fe (bcc)	0	33.75 ± 0.74	0.07 ± 0.057	0.2861 ± 0.01431
Si (fcc)	0	23.03 ± 0.96	0.00 ± 0.117	0.5351 ± 0.0267
$Fe_{90}Si_{10}$ (bcc)	15	25.46 ± 0.67	0.137 ± 0.014	0.4511 ± 0.0225
$Fe_{90}Si_{10}$ (bcc)	30	19.51 ± 0.03	0.236 ± 0.006	0.4528 ± 0.0226

downsizing of crystallite dimensions into the nanoscale regime.[31] Concomitantly, an escalation in lattice deformations is noted with prolonged milling time. These effects align with the mechanism postulated by Fecht et al.,[31] which identifies three distinct stages during MA. Firstly, deformation is localized within shear bands. Secondly, small-angle grain boundaries emerge, delineating individual grains. Finally, large-angle boundaries manifest, characterized by a fully random orientation of sizeable grains.

Table II outlines the evolution of the lattice parameter during the milling process. The initial lattice parameter, measured before milling, was 0.2861 nm. After 15 h of milling, a steady increase is observed, reaching 0.4511 nm. Following 30 h of milling, a further increase is noted, with the lattice parameter reaching 0.4528 nm. This expansion is attributed to the order–disorder transition induced by mechanical milling.

The increasing intensity of the (110) peak, as shown in Fig. 1, during the milling process indicates the diffusion of Si atoms within the Fe lattice, promoting the formation of a solid solution of Fe(Si).[32] These changes in the lattice parameter emphasize the structural transformations at the atomic level, highlighting the influence of mechanical milling on the order and arrangement of atoms within the material.

By comparing the experimental results of lattice parameters of FeSi solid solution with Vegard's law,[33]

$$a_{\text{alloy}} = x a_A + (1 - x) a_B \qquad (4)$$

In this context, a_A, a_B, and a_{alloy} represent the lattice parameters of pure A, pure B, and the alloy $A_x B_{(1-x)}$, respectively, where x is the fraction of one component in the alloy.

The lattice parameters of the FeSi solid solution, calculated using Eq. 4, are depicted in Fig. 2. The segregation profile of silicon is notably influenced by the cooling rate. Within the iron lattice, silicon occupies sites, augmenting strength through solid solution reinforcement, thereby impeding dislocation sliding. Extensive research has explored the impact of varying silicon concentrations on the deformation behavior of ferrite single crystals, leading to a natural decrease in deformability.[34] Deviation from Vegard's law is a common observation across diverse material classes, including oxides, ionic salts, and intermetallic compounds.

Such deviations often arise from structural phenomena, such as incomplete randomness in site occupancies, distortions like long-range ordering or clustering,[35] or variations in bond distances, indicating alterations in the material's electron configuration.[36,37] Vegard's law assumes a linear relationship between the lattice parameter and the composition of a solid solution. However, the experimental results for the $Fe_{90}Si_{10}$ nanostructured alloy deviate from Vegard's law. This deviation can be attributed to the following factors:

- Failure to satisfy the Hume–Rothery rules, which describe the conditions for obtaining a perfect solid solution. Specifically, in our case:
- The constituent elements have different crystal structures.
- There are significant differences in the atomic sizes of Fe (iron) and Si (silicon).

Additionally, we observed bowing parameters due to an increase in repulsive forces between the atoms in the alloy. This indicates that the interactions between Fe and Si atoms do not follow the linear behavior predicted by Vegard's law, leading to deviations in the expected lattice parameters.

Morphological Analysis

Figure 3 presents SEM micrographs illustrating nanostructured FeSi samples exposed to varying milling durations, demonstrating a noticeable reduction in mean particle size with increased processing time. The particle size, analyzed for Fig. 3a, b, and c using ImageJ software, decreased from 70 µm for unmilled powder to about 22 µm after 15 h of milling, further reducing to about 10 µm after 30 h of milling. Mechanical deformation occurs in the powder particles during milling, involving cycles of cold welding, fracturing, and subsequent re-welding.[38] This dynamic evolution, evident in the micrographs, emphasizes the influence of milling duration on the nanostructure of the FeSi samples. The morphological evolution of the $Fe_{90}Si_{10}$ alloy powder during mechanical alloying is shown in Fig. 3, revealing different morphologies at various milling stages. Initially, the $Fe_{90}Si_{10}$ mixture powder consisted of coarse particles with a mean size of 70 µm. After 15 h of milling (Fig. 3b), the mean particle size was reduced to 22 µm with irregular and isotropic shapes due to intensive fracture and cold welding. However,
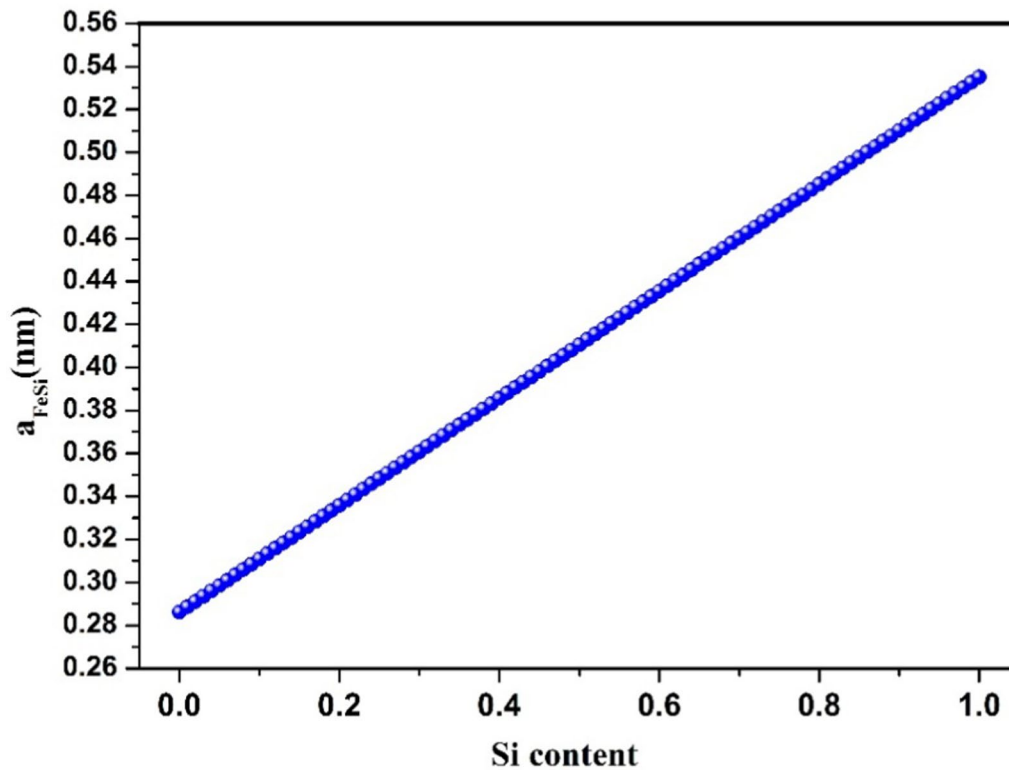
Fig. 2 Variation of the lattice parameters of the FeSi solid solution, obtained using Vegard law.

severe fracturing and agglomeration were observed in many studies due to the chaotic nature of mechanical alloying.[11,39] After 30 h of milling, the dominant morphology was platelet-shaped, with some round particles measuring about 10 μm in diameter (Fig. 3c). Some particles exhibited a layered structure of superposed Si and Fe layers, indicating ongoing mechanical alloying progress and particle size refinement. These results align with observations in mechanical alloying of ductile or brittle elements by other researchers.[40,41]

In Fig. 3d, e, and f, we present the EDS analysis results for the nanostructured $Fe_{90}Si_{10}$ alloy. These findings closely mirror the initial elemental composition of the $Fe_{90}Si_{10}$ powder mixture. The EDS spectrum of the unmilled mixture in Fig. 3d shows iron and silicon compositions of 94.4 wt.% and 5.6 wt.%, respectively. After 15 h of milling, as shown in Fig. 3e, the EDS spectrum of the FeSi mixture reveals iron and silicon compositions of 92 wt.% and 8 wt.%, respectively. However, after 30 h of milling, displayed in Fig. 3f, the EDS results show iron and silicon composition of 90.52 wt.% and 9.48 wt.%, respectively.

This indicates a change in the stoichiometry of the FeSi mixture during grinding, progressing from an unmilled mixture of 90 wt.% pure iron and 10 wt.% pure silicon to the formation of the $Fe_{90}Si_{10}$ alloy with complete diffusion of Si atoms into the iron. Notably, the EDS spectra exhibit only peaks corresponding to the elements present in the powders, indicating the alloy's uniformity and the absence of impurities or contamination introduced during grinding, including potential influences from the surrounding atmosphere, grinding balls, and internal jar walls. The agreement between the EDS and XRD results, coupled with the absence of extraneous peaks, enhances confidence in the reliability and purity of the nanostructured $Fe_{90}Si_{10}$ alloy obtained through milling.[42,43]

Figure 4 illustrates the EDS mapping of FeSi alloys before and after the milling process. The unmilled samples, as depicted in Fig. 4a, reveal a non-homogeneous distribution of the elements Fe and Si, as highlighted by the mapping analysis. This non-homogeneous distribution is likely due to a 1-h milling period without milling balls, which could have resulted in uneven mixing of the elements.

Upon increasing the milling time to 30 h, as shown in Fig. 4b, the EDS maps demonstrate a striking change. The distribution of Fe and Si becomes nearly identical, falling within the error limit of this analytical method. This result strongly suggests that the two elements have undergone extensive alloying, leading to the formation of the FeSi solid solution. This observation is consistent with the findings from x-ray diffraction analysis, which further confirms the successful formation of the FeSi solid solution in the milled samples.[44]
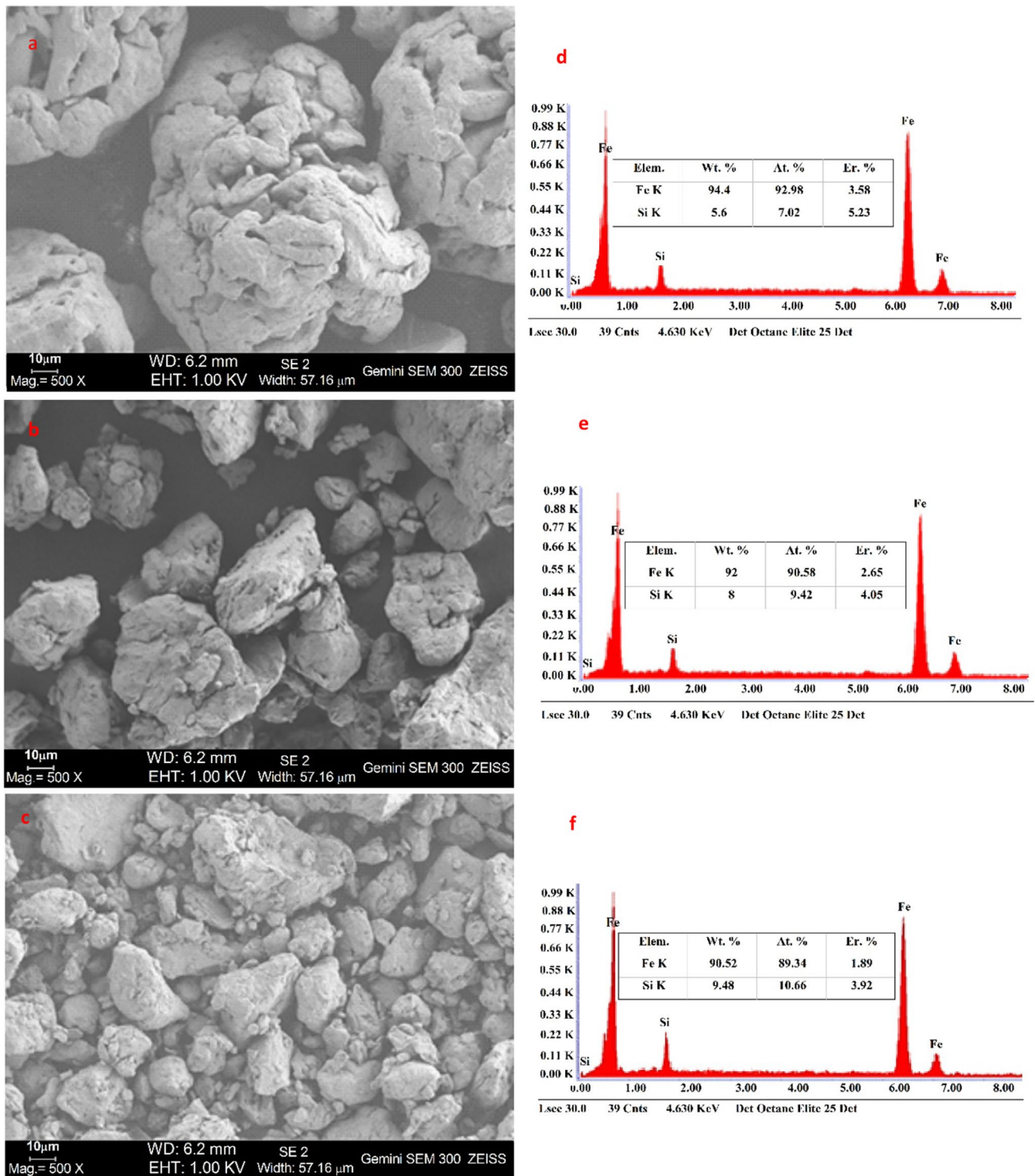
Fig. 3 SEM micrographs and EDS analyses of Fe$_{90}$Si$_{10}$ powder mixtures at different milling durations: (a) SEM micrograph at 0 h, (b) SEM micrograph at 15 h, (c) SEM micrograph at 30 h, (d) EDS analysis at 0 h, (e) EDS analysis at 15 h, and (f) EDS analysis at 30 h

Magnetic Properties

Prior to VSM analysis, it is critical to demagnetize all samples to eliminate remanence by gradually applying a reverse magnetic field. The most effective demagnetization method is the electrical method using alternating current (AC), which generates heat in the material, causing the atoms within the magnet to vibrate more vigorously. This
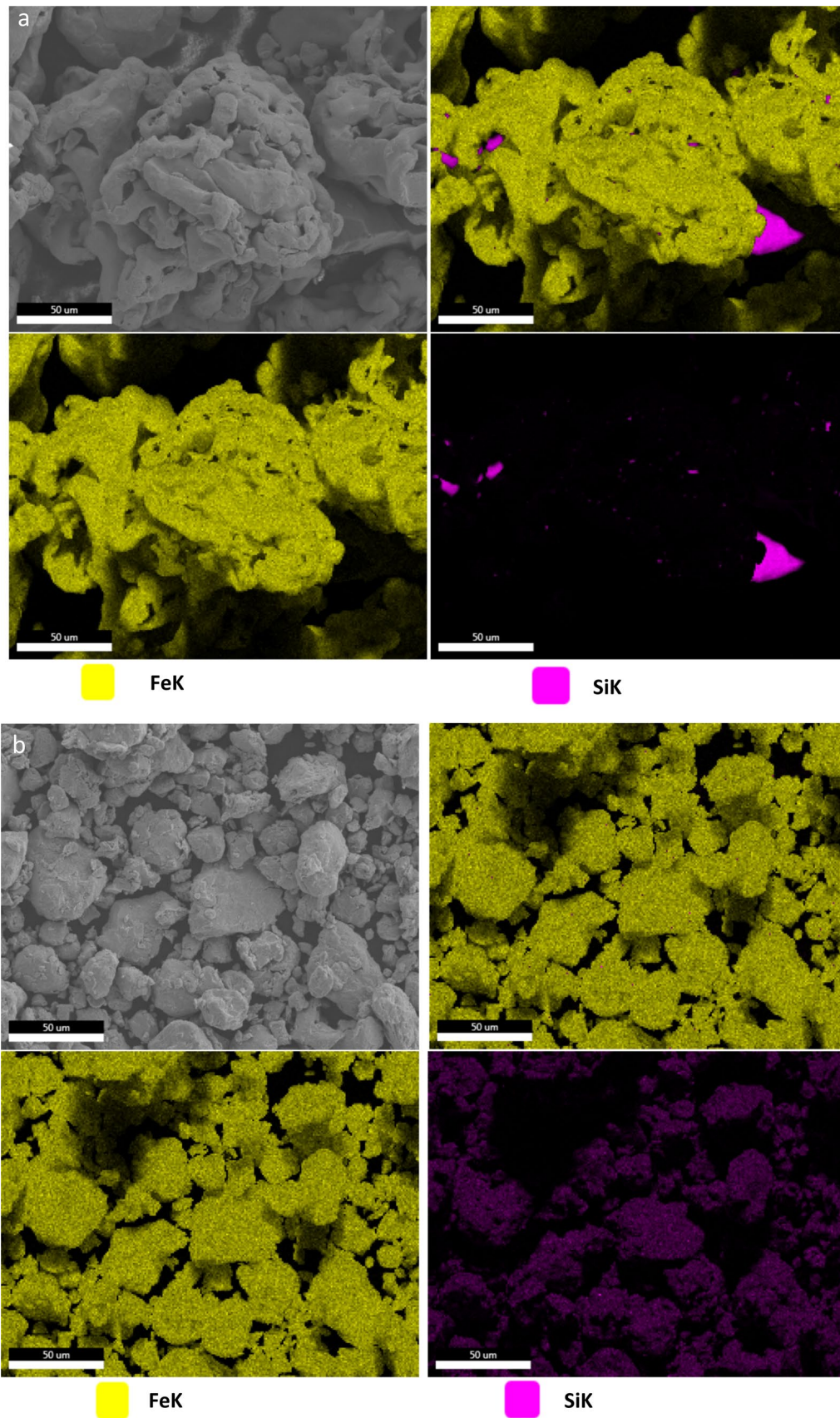
Fig. 4 (a) EDS elemental distribution maps of FeSi alloys prior to milling. (b) EDS elemental distribution maps of nanostructured FeSi milled for 30 h.

increased vibration disrupts the alignment of the magnet's domains, effectively demagnetizing the sample. Figure 5 displays the demagnetization curve of nanostructured FeSi milled at various durations. Additionally, DC-demagnetization (DCD), also known as reverse remanence, depicts the remanent field as a function of the previously applied field. The DCD measurement procedure involves saturating the sample in the maximum negative field, followed by the application and removal of a small positive field to measure and plot the magnetization (at zero field) against the previously applied positive field. This process is repeated with progressively larger positive fields until the resulting remanent magnetization is constant and equal to the remanence after saturation.[45–47]

Magnetization–hysteresis (M–H) loops at room temperature were measured for samples milled for various durations using a vibrating sample magnetometer. Figure 6 illustrates the M–H loops of the Fe$_{90}$Si$_{10}$ powders milled for different time periods, with the inset providing an expanded view of the curves near the origin. The hysteresis loops shown in Fig. 6 are characteristic of soft magnetic materials. The saturation magnetization (M_s) at an applied field of 15 kOe exhibits a gradual increase in powders milled for longer durations. Despite this increase, all samples exhibit ferromagnetic behavior, characterized by the presence of small magnetic domains, indicative of their soft ferromagnetic nature. This behavior is attributed to micro-distortions within the particles, resulting from extensive plastic deformation during the mechanical milling process. The observed trend in M_s is consistent with the observations in Tables I and II, where a decrease in crystallite size and an increase in lattice strain were noted. These interconnected factors collectively contribute to the change in M_s, highlighting the intricate relationship between structural modifications and magnetic properties in these nanostructured alloys. Furthermore, the presence of small magnetic domains suggests the presence of superparamagnetic behavior, which is typical in nanostructured materials and further supports the soft ferromagnetic nature of the samples.

Table III summarizes key magnetic parameters extracted from hysteresis curves shown in Fig. 6, including H_c, M_s, M_r, and M_r/M_s. The M_s values in Table III display significant variation, notably increasing from 87.73 emu/g to 159.27 emu/g after 30 hours of milling.[48,49] This rise in M_s indicates improved magnetic properties due to structural changes induced by milling, such as grain refinement and increased lattice strain. These modifications enhance the magnetic behavior of nanostructured FeSi alloys, showcasing the effectiveness of mechanical milling in tailoring their magnetic properties. The increase in M_s is mainly attributed to the incorporation of diamagnetic Si atoms near Fe atoms, influencing iron's magnetic moment. The heightened M_s
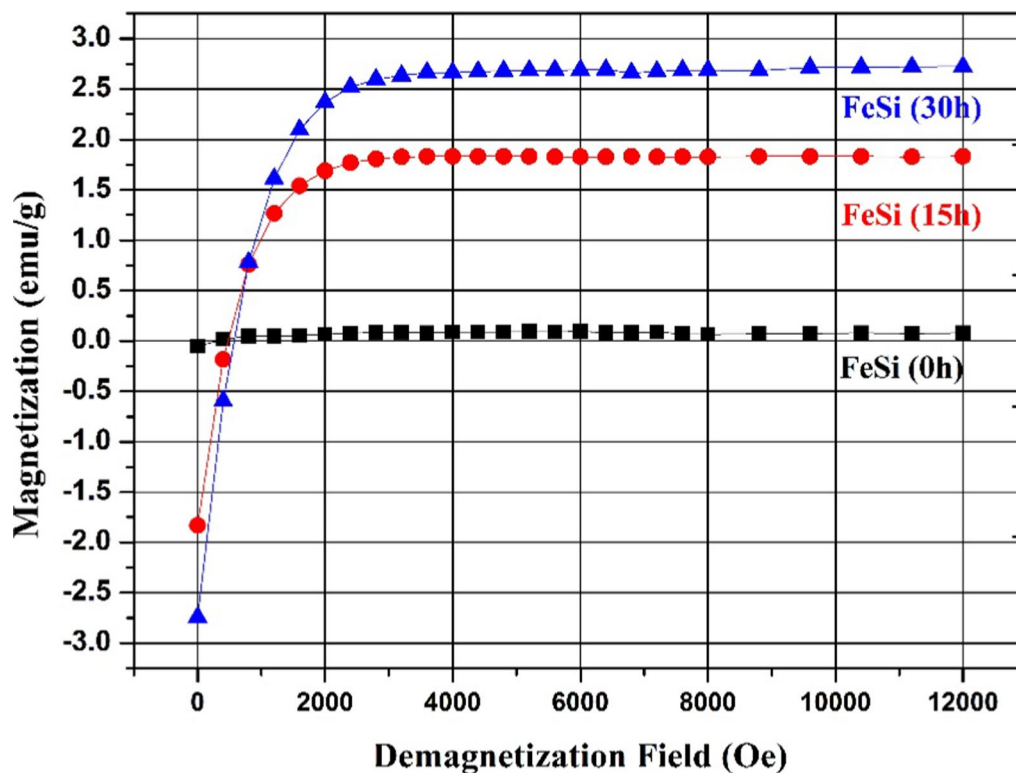

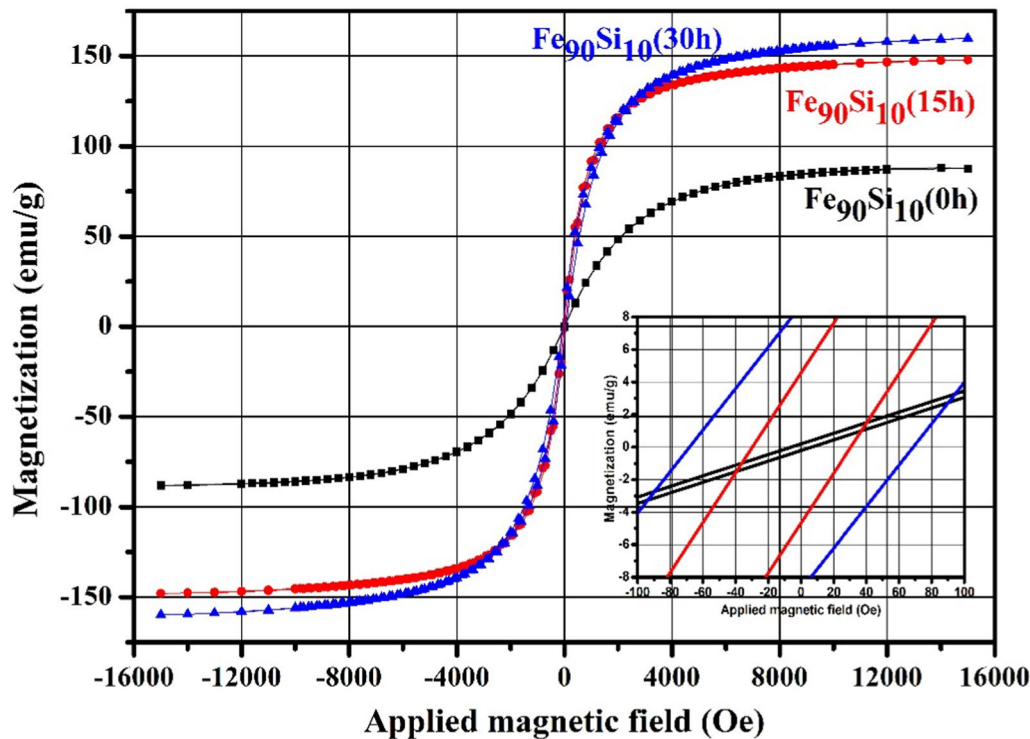**Fig. 5** Intrinsic demagnetization curve of the nanostructured FeSi alloy.

Fig. 6 Hysteresis curves of $Fe_{90}Si_{10}$ powder samples milled for 0, 15, and 30 h at room temperature.

Table III Magnetic parameters of nanostructured $Fe_{90}Si_{10}$ alloy milled for various durations

Milling time (h)	H_c (Oe)	M_r (emu/g)	M_s (emu/g)	M_s/M_s
0	8.13 ± 0.406	0.20 ± 0.01	87.73 ± 4.386	0.002 ± 0.0001
15	30.60 ± 1.530	4.58 ± 0.229	147.56 ± 7.378	0.031 ± 0.0018
30	68.98 ± 3.449	8.72 ± 0.436	159.27 ± 7.963	0.054 ± 0.0032

is also notable for its reduced magneto-crystalline anisotropy, facilitating easier spin rotation.[50] The lower saturation magnetization value observed in the unmilled powders with 90% Fe raises questions about the distinctive magnetic characteristics of these powders and highlights the intricate relationship among composition, milling duration, and magnetic properties.

This discrepancy is explained by the dynamic interaction between Fe and Si atoms within the solid solution, where the initial reduction in M_s due to the diamagnetic influence of Si is overcome by the subsequent formation of the Fe(Si) solid solution, leading to an overall increase in M_s. This enhancement in M_s is attributed to various factors, including changes in magnetic ordering, electronic configuration, or spin alignment resulting from Si incorporation into the Fe lattice. Further understanding of these mechanisms can be obtained from additional details in the study or relevant literature.[10]

The observed increase in H_c can be attributed to the irreversible displacement of magnetic domain walls, induced by various types of defects such as alterations in microstructure, grain boundaries, internal strain, and dislocations. This increase in H_c reflects heightened magnetic anisotropy, especially at the beginning of the milling process.[51,52] However, it is important to note that several factors can influence H_c. Lattice strain, along with potential underestimations in grain size and uniformity, can collectively affect coercivity. Research by Li et al.[53] highlights that grain size, grain size distribution, and grain boundary chemistry significantly impact coercivity. Additionally, defects such as dislocations, grain boundaries, inclusions, and voids can contribute to H_c. In polycrystalline materials, the interaction of domain walls with grain boundaries plays a crucial role in H_c. As grain size decreases, the larger volume fraction of grain boundaries leads to increased H_c due to the hindering effect on domain wall (Bloch wall) motion.[54] It is important to note that magneto-crystalline anisotropy also affects H_c.[55,56]

Moreover, the variations in M_r and M_r/M_s across different milling durations, as delineated in Table III, provide valuable insights into the material's resistance to demagnetization.

The remanence and squareness of FeSi surpass those of pure Fe owing to the incorporation of Si atoms into the alloy. Upon Si integration into the Fe lattice, localized magnetic moments with opposite directions to the Fe moments are created. This induces a decrease in the net magnetic moment of the Fe atoms, resulting in an overall reduction in the alloy's magnetization. However, the existence of these Si-induced moments in FeSi concurrently contributes to an augmentation in magnetization remanence. These moments exhibit a tendency to align with the external magnetic field and retain their orientation even after the field is withdrawn. The magnetization remanence of FeSi exhibits variability with changes in Si content. With an initial increase in Si content, the magnetization remanence experiences a rise due to the aforementioned effect of Si-induced moments. Nevertheless, at higher Si concentrations, the magnetization remanence begins to decline. This decline is attributed to the interference of diamagnetic Si ions, which disrupt the ferromagnetic ordering of the Fe ions, leading to an overall reduction in the alloy's magnetic moment. Consequently, the fluctuation in Si content emerges as a significant factor influencing the magnetization remanence of FeSi.[57–59]

Conclusions

The successful synthesis of nanostructured Fe₉₀Si₁₀ through ball milling from elemental Fe and Si powders was achieved, with significant findings revealed through SEM, XRD, and VSM analyses. XRD results indicated the formation of a (bcc) α-Fe(Si) solid solution, evolving through Si diffusion within the Fe lattice, with the lattice parameter increasing to 0.4528 nm after 30 h, accompanied by a reduction in crystallite size and an increase in lattice strain. The morphological evolution of the Fe₉₀Si₁₀ alloy displayed diverse shapes, transitioning from coarse particles to smaller, nearly spherical shapes, with some exhibiting layered Si and Fe structures, suggesting continued mechanical alloying and particle size refinement. The average particle size reduced from approximately 70 μm for the unmilled powders to around 10 μm after 30 h. EDS analysis confirmed the presence of all elements without any detectable impurities. The variations in magnetic properties were attributed to microstructural changes, specifically the concentration of atoms at particle and grain boundaries. The increase in M_s was linked to the presence of diamagnetic silicon (Si) atoms, which affected iron's magnetic moment and decreased magneto-crystalline anisotropy. Elevated H_c, M_r, and M_r/M_s values were associated with the irreversible movement of magnetic domain walls induced by defects, highlighting heightened magnetic anisotropy in the material. This study provides valuable insights into the relationship between milling duration, structural properties, and magnetic behavior in nanostructured Fe₉₀Si₁₀ alloys, offering potential advancements in magnetic materials for various applications.

References

1. L. Abbassi, D. Mesguich, L. Coulomb, G. Chevallier, R. Aries, C. Estournès, E. Flahaut, R. Viennois, and M. Beaudhuin, In-situ reactive synthesis of dense nanostructured β-FeSi₂ by spark plasma sintering. *J. Alloys Compd.* 902, 163683 (2022).
2. Paras, K. Yadav, P. Kumar, D. R. Teja, S. Chakraborty, M. Chakraborty, S.S. Mohapatra, A. Sahoo, M.M.C. Chou, C.T. Liang, D. R. Hang, A review on low-dimensional nanomaterials: nanofabrication, characterization and applications. *Nanomaterials* 13, 160 (2022).
3. A. Nozariasbmarz, P. Roy, Z. Zamanipour, J.H. Dycus, M.J. Cabral, J.M. LeBeau, J.S. Krasinski, and D. Vashaee, Comparison of thermoelectric properties of nanostructured Mg₂Si, FeSi₂, SiGe, and nanocomposites of SiGe-Mg₂Si, SiGe-FeSi₂. *APL Mater.* 4, 104814 (2016).
4. S. Wu, Y. Dong, X. Li, M. Gong, R. Zhao, W. Gao, H. Wu, A. He, J. Li, X. Wang, and X. Liu, Microstructure and magnetic properties of FeSiCr soft magnetic powder cores with a MgO insulating layer prepared by the sol-gel method. *Ceram. Int.* 48(15), 22237 (2022).
5. A.V. Rane, K. Kanny, V.K. Abitha, S. Thomas, Chapter 5: Methods for synthesis of nanoparticles and fabrication of nanocomposites. in *Micro and Nano Technologies, Synthesis of Inorganic Nanomaterials, Woodhead Publishing*, 2018, pp 121–139. ISBN 9780081019757, https://doi.org/10.1016/B978-0-08-101975-7.00005-1.
6. A. Valizadeh and S. Mussa Farkhani, Electrospinning and electrospun nanofibres. *IET Nanobiotechnol.* 8, 59 (2014). https://doi.org/10.1049/iet-nbt.2012.0040
7. M. Pérez-Page, E. Yu, J. Li, M. Rahman, D.M. Dryden, R. Vidu, and P. Stroeve, Template-based syntheses for shape controlled nanostructures. *Adv. Coll. Interface. Sci.* 234, 51 (2016).
8. M. Ouadah and A. Younes, Effects of silicon concentration on the magnetic and structural properties of nanostructured Fe-Si alloy synthesized by ball mill process. *Int. J. Adv. Manuf. Technol.* 127, 3655 (2023).
9. L. Faghi, S. Triaa, F. Siahmed, and M. Azzaz, Synthesis and characterization of nanocrystalline Fe-40 at.% Si alloy prepared by high energy ball milling. *Int. J. Mater. Res.* 105(1), 32–38 (2014).
10. E.P. Yelsukov and G.A. Dorofeev, Mechanical alloying in binary Fe-M (M= C, B, Al, Si, Ge, Sn) systems. *J. Mater. Sci.* 39(16–17), 5071 (2004).
11. D. Guo, G. Xie, and J. Luo, Mechanical properties of nanoparticles: basics and applications. *J. Phys. D Appl. Phys.* 47(1), 013001 (2013).
12. A. Younes and N. Kherrouba, Eddy current and magnetic evaluation of nanostructured iron–cobalt produced by ball-milling. *Emerg. Mater. Res* 11(2), 268 (2022).

13. C. Koch, Synthesis of nanostructured materials by mechanical milling: problems and opportunities. *Nanostruct. Mater.* 9(1–8), 13 (1997).

14. A.F. Manchón-Gordón, A. Gómez, J.J. Ipus, J.S. Blázquez, C.F. Conde, and A. Conde, Milling effects on the distribution of Curie temperatures and magnetic properties of Ni-doped La0·7Ca$_{0.3}$MnO$_3$ compounds. *J. Alloys Compd.* 848, 156566 (2020).

15. A.F. Manchón-Gordón, J.J. Ipus, J.S. Blázquez, C.F. Conde, and A. Conde, Influence of milling time on the homogeneity and magnetism of a Fe$_{70}$Zr$_{30}$ partially amorphous alloy: distribution of curie temperatures. *Materials* 13, 490 (2020).

16. J. Wang, S. Song, H. Sun, and Z. Xue, Improvement of magnetic properties for FeSi/FeSiAl compound soft magnetic composites by introducing impact of powder size matching. *J. Mater. Sci. Mater. Electron.* 32, 8545 (2021).

17. A.R. Balakrishna and R.D. James, A tool to predict coercivity in magnetic materials. *Acta Mater.* 208, 116697 (2021).

18. M. Dascalu, F. Cesura, G. Lev, O. Diéguez, A. Kohn, and I. Goldfarb, Controlling the supermagnetic response of tetragonal α-FeSi$_2$ nanoislands. *Appl. Surf. Sci.* 476, 189 (2019).

19. V.A. Du, A. Sidorenko, O. Bethge, S. Paschen, E. Bertagnolli, and U. Schubert, Iron silicide nanoparticles in a SiC/C matrix from organometallic polymers: characterization and magnetic properties. *J. Mater. Chem.* 21(33), 12232 (2011).

20. G. Ouyang, X. Chen, Y. Liang, C. Macziewski, and J. Cui, Review of Fe-6.5 wt.% Si high silicon steel: a promising soft magnetic material for sub-kHz application. *J. Magn. Magn. Mater.* 481, 234–250 (2019).

21. J.M. Silveyra, E. Ferrara, D.L. Huber, T.C. Monson, Soft magnetic materials for a sustainable and electrified world. *Science* 362(6413), eaao0195 (2018).

22. F. Fiorillo, G. Bertotti, C. Appino, M. Pasquale. Soft magnetic materials. In *Wiley Encyclopedia of Electrical and Electronics Engineering* (pp. 1–42) (2016). Wiley.

23. A. Krings, A. Boglietti, A. Cavagnino, and S. Sprague, Soft magnetic material status and trends in electric machines. *IEEE Trans. Ind. Electron.* 64(3), 2405 (2016).

24. C. Suryanarayana and A. Inoue, Iron-based bulk metallic glasses. *Int. Mater. Rev.* 58(3), 131 (2013).

25. Y.G. Yoo, S.C. Yu, and J.M. Greneche, The structural and magnetic properties of Fe-Si and Fe-C solid solutions as a function of milling times. *J. Mater. Sci.* 39, 5523 (2004).

26. M. Khajepour and S. Sharafi, Characterization of nanostructured Fe-Co-Si powder alloy. *Powder Technol.* 232, 124 (2012).

27. T. Clark and S.N. Mathaudhu, Microstructure and magnetic properties of dilute nanocrystalline Fe-Si prepared by high energy ball milling. *J. Magn. Magn. Mater.* 484, 350 (2019).

28. R.R. Rodriguez, G.A. Perez-Alcazar, H. Sanchez, M. Sacilotti, and J.M. Greneche, Magnetic and structural properties of the nanostructured Fe$_{1-x}$Si$_x$ system with x = 0.1, 0.2 and 0.3, mechanical alloyed and sintered. *Phys. Status Solidi C* 4(11), 4220 (2007).

29. A. Abada, A. Younes, and A. Manseri, Magnetic and structural properties of nanostructured FeSn, FeSnTi, FeSnV and FeSnTiV alloys elaborated via ball milling process. *J. Korean Phys. Soc.* 84, 33 (2024).

30. A. Younes, R. Amraoui, A. Manseri, and F. Smaili, The impact of Cu, Ni and Fe$_2$O$_3$ on the magnetic behavior and structural properties of FeSiO$_2$ nanocomposite synthesized through ball milling. *Phys. Scr.* 98, 115536 (2023).

31. H.J. Fecht, Synthesis and properties of nanocrystalline metals and alloys prepared by mechanical attrition. *Nanostruct. Mater.* 1(2), 125 (1992).

32. Z. Bensebaa, B. Bouzabata, and A. Otmani, Study of nanocrystalline FeSi alloys prepared by mechanical alloying. *J. Alloys Compd.* 469(1–2), 24 (2009).

33. R.E. Bailey and S. Nie, Alloyed semiconductor quantum dots: tuning the optical properties without changing the particle size. *J. Am. Chem. Soc.* 125(23), 7100 (2003).

34. L. Horbach, C. Gebhardt, J. Zhang, B.D. Joseph, A. Bührig-Polaczek, and C. Broeckmann, The effect of silicon microsegregation on the mechanical properties of high silicon alloyed ductile cast iron under monotonous loading. *Heliyon* 10, e23904 (2024).

35. M. Castellanos and A.R. West, Deviations from Vegard's law in oxide solid solutions: the systems Li$_2$ TiO$_3$-MgO and Li$_2$ TiO$_3$-Na$_2$TiO$_3$. *J. Chem. Soc. Faraday Trans.: Phys. Chem. Condens. Phases* 76, 2159 (1980).

36. S. Le Tonquesse, M. Pasturel, V. Demange, A. Tayal, P.L. Solari, and C. Prestipino, X-ray absorption study on the origin of the deviation from Vegard's law for U (Al$_{1-x}$Ge$_x$)$_3$ solid solution. *J. Nucl. Mater.* 526, 151772 (2019).

37. C. Xu, C.L. Senaratne, J. Kouvetakis, and J. Menendez, Experimental doping dependence of the lattice parameter in n-type Ge: identifying the correct theoretical framework by comparison with Si. *Phys. Rev. B* 93(4), 041201 (2016).

38. C. Suryanarayana, Mechanical alloying and milling. *Prog. Mater. Sci.* 46(1–2), 1 (2001).

39. H. Gökçe and M.L. Öveçoğlu, Microstructure-property evolution of mechanically alloyed Al-20 wt.% Si matrix powders and sintered composites reinforced withTiB2 particulates. *Eng. Sci. Technol. Int. J.* 39, 101341 (2023).

40. N. Guemmoud, A. Hafs, and T. Hafs, Effect of milling time on the structural, microstructure, and magnetic properties of nanocrystalline Fe$_{90}$Sb$_{10}$ powders obtained by high-energy ball milling. *Int. J. Adv. Manuf. Technol.* 122, 2043 (2022).

41. T. Aida, T. Kawai, M. Ohtake, M. Futamoto, F. Kirino, and N. Inaba, Effect of Si/Fe composition, substrate temperature, and substrate orientation on the structure and magnetic properties of Fe-Si alloy film. *J Magn Soc Jpn* 40, 95 (2016).

42. P. Banerjee, N.S. Kumar, A. Franco Jr., A.K. Swain, and K. Chandra Babu Naidu, Insights into the dielectric loss mechanism of bianisotropic FeSi/SiC composite materials. *ACS Omega* 5(40), 25968 (2020).

43. C.L. Yeh, K.T. Chen, and T.H. Shieh, Effects of Fe/Si stoichiometry on formation of Fe$_3$Si/FeSi-al$_2$o$_3$ composites by aluminothermic combustion synthesis. *Metals* 11(11), 1709 (2021).

44. Y. Sun, Y. Chen, C. Lan, Y. Tan, L. Zhang, B. Dong, and S. Lan, Microstructure, particle size, and magnetic property of Fe-6.5 wt.% Si nanocrystalline alloys prepared by mechanical alloying. *JOM* 76, 1066 (2024). https://doi.org/10.1007/s11837-023-06300-9.

45. T. Mohri, Y. Chen, M. Kohyama, S. Ogata, A. Saengdeejing, S. Kumar Bhattacharya, M. Wakeda, S. Shinzato, and H. Kimizuka, Mechanical properties of Fe-rich Si alloy from Hamiltonian. *npj Comput Mater* 3, 10 (2017).

46. X. Liu, Y. Li, Z. Liu, and Z. Zhang, Performance evaluation of a permanent magnet-assisted synchronous reluctance machine with hybrid magnets of ferrite magnets and rare-earth PMs. *Int. J. Appl. Electromagnet Mech* 56, 413 (2018).

47. M.P.C. Kalita, A. Perumal, and A. Srinivasan, Structure and magnetic properties of nanocrystalline Fe$_{75}$Si$_{25}$ powders prepared by mechanical alloying. *J. Magn. Magn. Mater.* 320, 2780 (2008).

48. Z. Guo, J. Wang, W. Chen, D. Chen, H. Sun, Z. Xue, and C. Wang, Crystal-like microstructural Finemet/FeSi compound powder core with excellent soft magnetic properties and its loss separation analysis. *Mater. Des.* 192, 108769 (2020).

49. N.R. Overman, X. Jiang, R.K. Kukkadapu, T. Clark, T.J. Roosendaal, G. Coffey, J.E. Shield, and S.N. Mathaudhu, Physical and electrical properties of melt-spun Fe-Si (3–8 wt %) soft magnetic ribbons. *Mater Charact* 136, 212 (2018).

50. D.M. Blanco, P. Gorria, and J.A. Blanco, Nanostructured Fe obtained by high-energy ball milling. *J. Magn. Magn. Mater.* 300, e339 (2006).
51. K.L. Alvarez, H.A. Baghbaderani, J.M. Martín, N. Burgos, P. McCloskey, J. González, and A. Masood, Novel predictive methodology of amorphisation of gas-atomised Fe-Si-B alloy powders. *J. Non-Cryst. Solids* 574, 121151 (2021).
52. J. Shen, B. Wang, L. Cai, L. Liu, C. Zhang, B. Wang, Y. Tian, Y. Yu, J. Dong, and G. Wang, Magnetic properties and thermal stability of Fe-based amorphous/carbonyl iron soft magnetic composites. *J. Mater. Sci. Mater. Electron.* 34, 1169 (2023).
53. M. Li, R. Birringer, W.L. Johnson, and R.D. Shull, Nanocrystalline Fe-Si phase by mechanical attrition and its soft magnetic properties. *Nanostruct. Mater.* 3, 407 (1993).
54. H. Vinzelberg, J. Schumann, D. Elefant, E. Arushanov, and O.G. Schmidt, Transport and magnetic properties of Fe$_3$Si epitaxial films. *J. Appl. Phys.* 104(9), 093707 (2008).
55. M.E. McHenry and D.E. Laughlin, Nano-scale materials development for future magnetic applications. *Acta Mater.* 48(1), 223 (2000).
56. J. Wang, Z. Guo, Q. Zeng, G. Hang, Z. Xue, D. Chen, Z. Liang, and H. Sun, Magnetic properties regulation and loss contribution analysis for Fe-based amorphous powder cores doped with micron-sized FeSi powders. *J. Magn. Magn. Mater.* 510, 166931 (2020).
57. M. Salaheldeen, A. Garcia-Gomez, P. Corte-Leon, A. Gonzalez, M. Ipatov, V. Zhukova, J. Gonzalez, R. Lopez Anton, and A. Zhukov, Manipulation of magnetic and structure properties of Ni$_2$FeSi glass-coated microwires by annealing. *J. Alloys Compd.* 942, 169026 (2022).
58. M. Hocine, A. Guittoum, M. Hemmous, D. Martínez-Blanco, P. Gorria, B. Rahal, and A. Laggoun, The role of silicon on the microstructure and magnetic behaviour of nanostructured (Fe$_{0.7}$Co$_{0.3}$)$_{100-x}$Si$_x$ powders. *J. Magn. Magn. Mater.* 422, 149 (2017).
59. M. Ouadah, A. Younes, O. Touhami, and R. Ibtiouen, Assessing the impact of magnetic circuit corrosion on the magnetic performance of induction machines. *Electr. Eng.* (2024). https://doi.org/10.1007/s00202-023-02203-9.